Supporting Information

Nitrogen Doped Fe_7S_8 as Highly Efficient Electrocatalysts for Hydrogen Evolution Reaction

Jian Ye[#1,2], Shuwen Niu[#3] , Leijie Zhang[1,4], Gongming Wang[3], Junfa Zhu[1,*]

[1] *National Synchrotron Radiation Laboratory, University of Science and Technology of China, Hefei 230029, China*
[2] *School of Science, Anhui Agricultural University, Hefei 230036, China*
[3] *Hefei National Laboratory for Physical Science at the Microscale, Department of Chemistry, University of Science and Technology of China, Hefei, Anhui 230026, China*
[4] *Specreation Instruments Co., Ltd., Hefei, 230026, P. R. China*

[*]Corresponding author.
E-mail address: jfzhu@ustc.edu.cn (J. F. Zhu)

Experimental

Sample preparation

The FeOOH sample was obtained by a facile solvothermal method. Firstly, 0.81 g $FeCl_3$ and 0.8 g NH_4Cl were put into 50 mL deionized water with strong agitation. After that, the above mixed solution was transferred into a Teflon-linked steel autoclave and keeped at 120 °C for 16 h to form FeOOH/CC sample. Then, this sample were further collected and annealed at 600 °C for 1 h in Ar to obtain FeS_2/CC via using sulfur powder as the sulfur source. Afterwards, the above sample was annealed at 600 °C under 50 sccm NH_3 for 1 h to obtain nitrogen doped Fe_7S_8 (N-Fe_7S_8).

Materials characterization

Morphologies and microstructures of FeS_2 and N-Fe_7S_8 were investigated by using Field emission scanning electron micro-scope (FESEM, Hitachi SU8010) and the transmission electron microscope (TEM, JEOL 2100F). X-ray diffraction (XRD) reactor with Cu Kα radiation (Rigaku D/Max-2550) was used to check their phase structure. The X-Ray photoelectron spectroscopy (XPS) spectra and the Fe L-edge NEXAFS experiments were performed at beamline BL10B in the Hefei Light Source of National Synchrotron Radiation Laboratory (NSRL) in Hefei, China. The Fe-K edge X-ray absorption fine structure (XAFS) spectra were obtained in transmission mode on Table XAFS-500 (Specreation Instruments Co., Ltd.).

Electrochemical measurements

HER performances of the working electrodes were conducted by using an electrochemical workstation (CH Instrument 660D) with a standard three-electrode setup at the temperature of 25 °C, where the carbon rod (D = 8 mm) and saturated calomel electrode (SCE) and were used as the counter electrode and reference electrode respectively. The 1 M KOH solution was used as the electrolyte. The conversion potential of E(RHE) was obtained according to Eq. (1).

$$E(RHE) = E(SCE) + 0.059 \times pH + 0.244 \quad (1)$$

The LSV curves were obtained at a scan rate of 5 mV s^{-1}. The Tafel curves were derived by LSV curves. The EIS spectra were obtained by testing at the initial voltage within a frequency range from 100 kHz to 0.01 Hz, where AC amplitude was set as 5 mV. The HER stability test was carried out by a continuous current test at 100 mA cm^{-2} for 100 h. These results were revised by IR-compensation. The TOF values were calculated using a previously reported method, where the number of active sites was estimated as the amount of surface sites (including N, Fe and S atoms)[1].

Density functional theory (DFT) calculations.

The DFT calculations were performed by using the CASTEP program implemented in the Materials Studios package of Accelrys Inc. The electron exchange-correlation potential was treated by Perdew–Burke–Ernzerhof functional (PBE) of generalized gradient approximation (GGA) method[2-3]. The plane-wave kinetic energy cutoff and self-consistent field tolerance were set to 500 eV and 1.0×10^{-6} eV/atom, respectively. The Brillouin zone was sampled by a 2×2×1 and 4×4×1 Monkhorst-Pack mesh k-points for surface structural optimization and density of states (DOS) calculations, respectively. The convergence criterions for geometry optimization were set to 1×10^{-5} eV/atom for energy, 0.03 eV/Å for maximum force and 1×10^{-3} Å for maximum displacement. DFT simulations were performed based on the crystal structures of cubic FeS_2 (a=b=c=5.4179 Å, JCPDS No.42-1340) with space group of Pa-3 and hexagonal Fe_7S_8 with the space group of P3121. The FeS_2 (001) surface was modeled by a periodic slab repeated in a 2×2 surface unit cell with a vacuum region of 15 Å between the slabs along the Z axis. The N-Fe_7S_8 (001) model was constructed by replacing a S atom with N in a pristine Fe_7S_8 (001). The H_2O absorption energy was calculated by the following equation, $\Delta E_{H_2O} = E_{surf\text{-}H_2O} - E_{surf} - E_{H_2O}$, where $E_{surf\text{-}H_2O}$ is the total energy of surface covered with a H_2O molecule, E_{surf}

is the energy of clean surface, and E_{H_2O} is the energy of a H_2O molecule in gas phase. A complete LST/QST approach was used to determine the transition state of water dissociation.

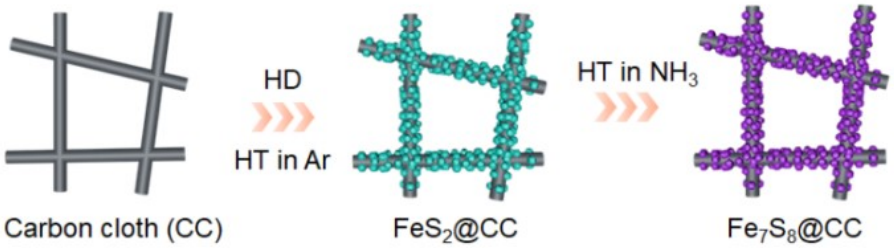

Scheme S1. Simplified schematics of the preparation process of N-Fe_7S_8/CC.

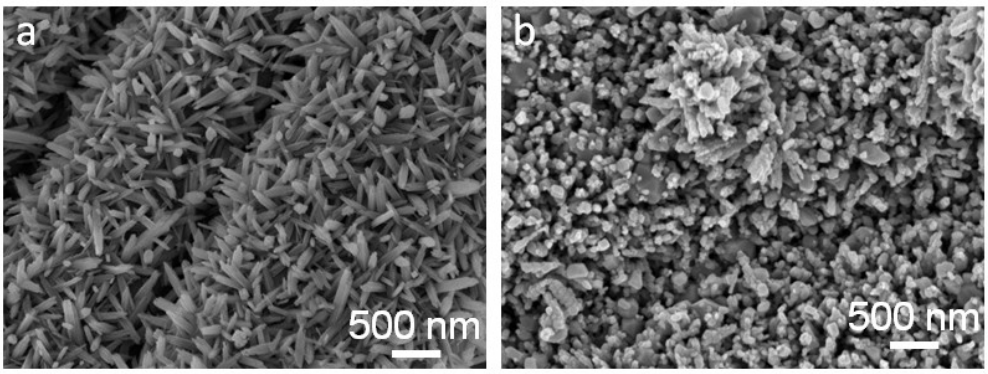

Figure S1. SEM images of (a) FeOOH and (b) N-Fe_xS_y-400.

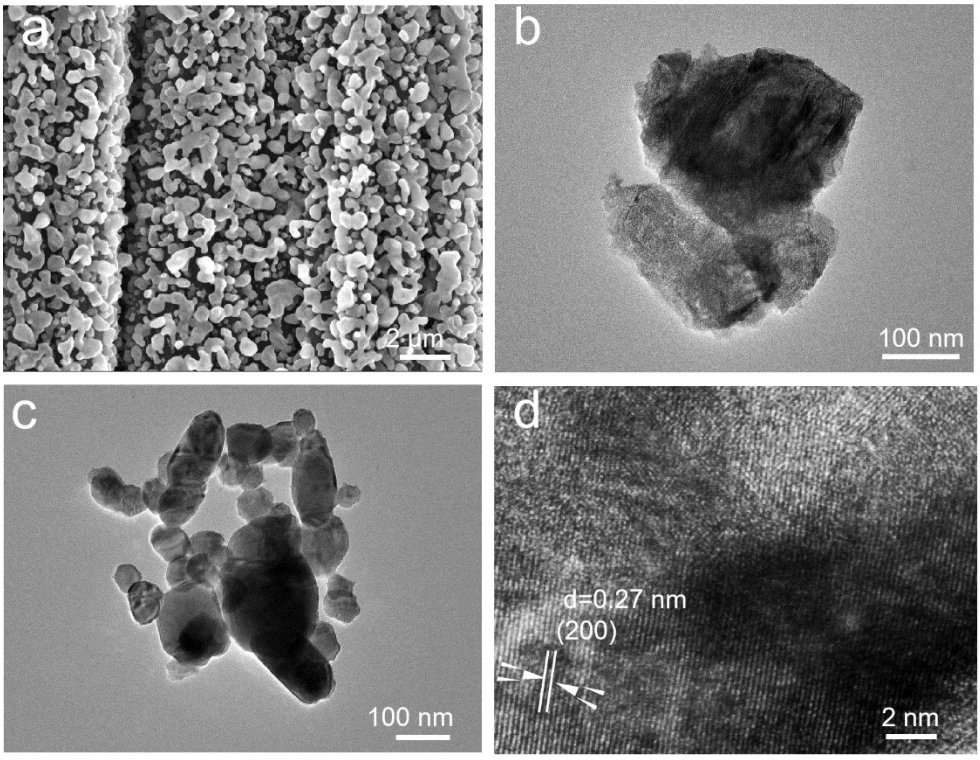

Figure S2. SEM-TEM images of (a, b) FeS_2 and (c) N-Fe_7S_8 samples. (d) HRTEM image of FeS_2 sample.

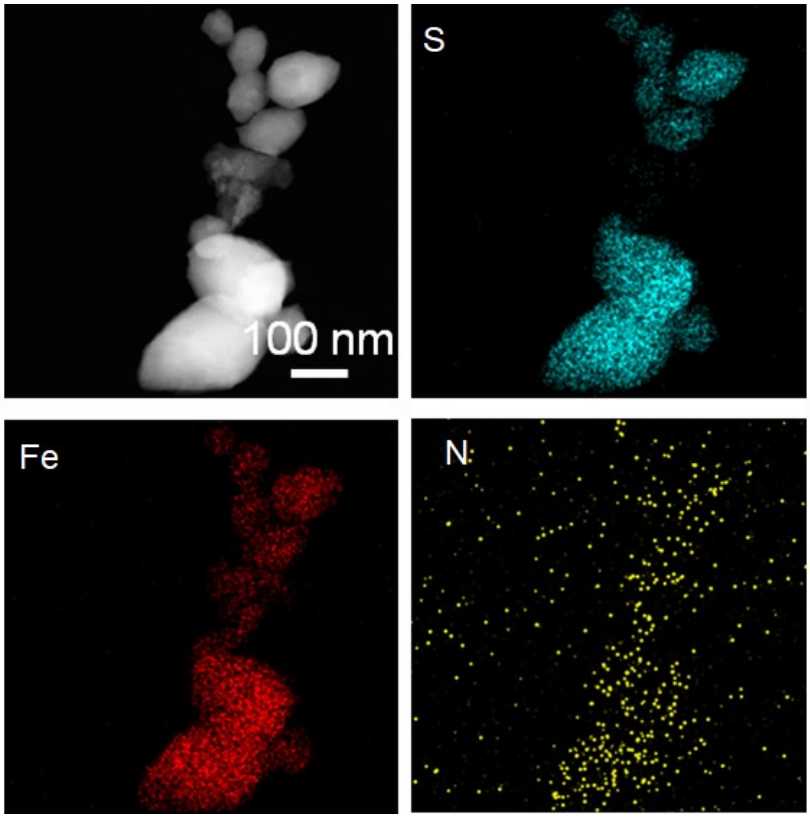

Figure S3. Elemental mapping images of the N-Fe_7S_8.

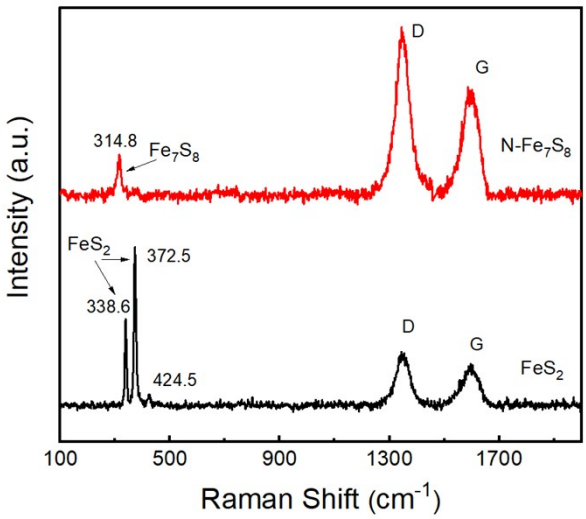

Figure S4. Raman spectra of FeS_2@CC and N-Fe_7S_8@CC.

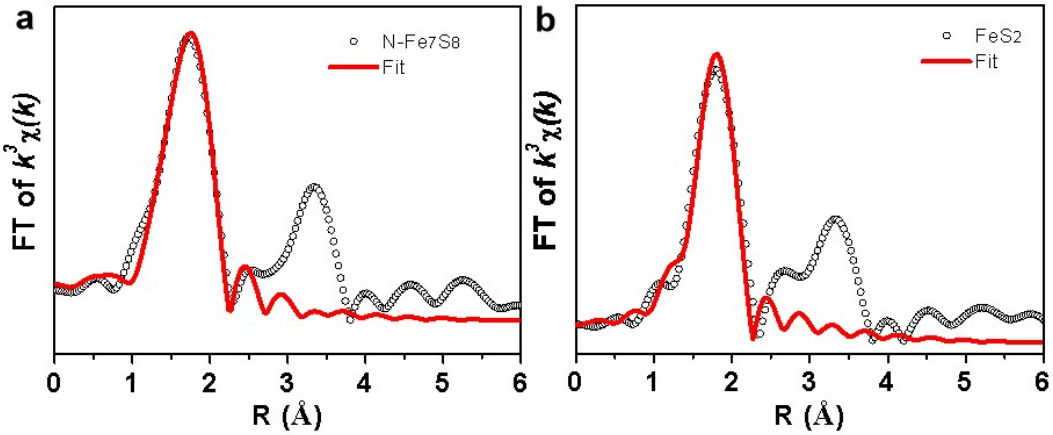

Figure S5. Extended X-ray absorption fine structure spectra and fits in R-space at the Fe K-edge of (a) N-Fe_7S_8 and (b) FeS_2

Table S1. EXAFS fitting parameters at the Fe K-edge of FeS_2 and N-Fe_7S_8 samples samples (S_0^2=0.83)

samples	path	C. N.[a]	R (Å) [b]	σ^2 ($\times 10^{-3}$ Å^2) [c]	ΔE (eV) [d]	R factor[e]
FeS_2	Fe-S	4.7	2.26	4.6	3.4	0.02
N-Fe_7S_8	Fe-N	0.2	2.01	7.7	7.1	0.02
	Fe-S	4.1	2.31	1.2		

[a]C. N.: coordination numbers; [b]R: bond distance; [c]σ^2: Debye-Waller factors; [d]ΔE_0: the inner potential correction. [e]R factor: goodness of fit.

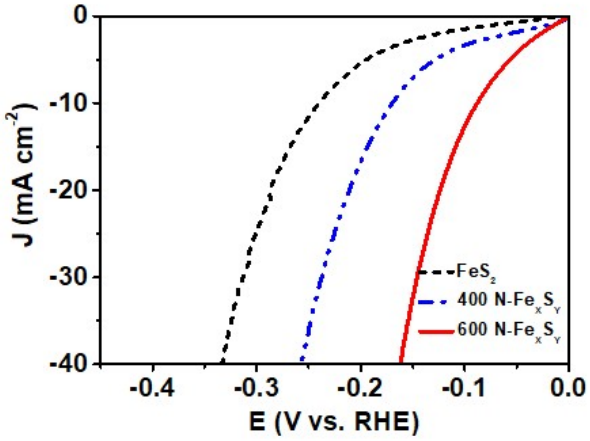

Figure S6. LSV curves FeS_2, N-FexSy-400 and N-FexSy-600.

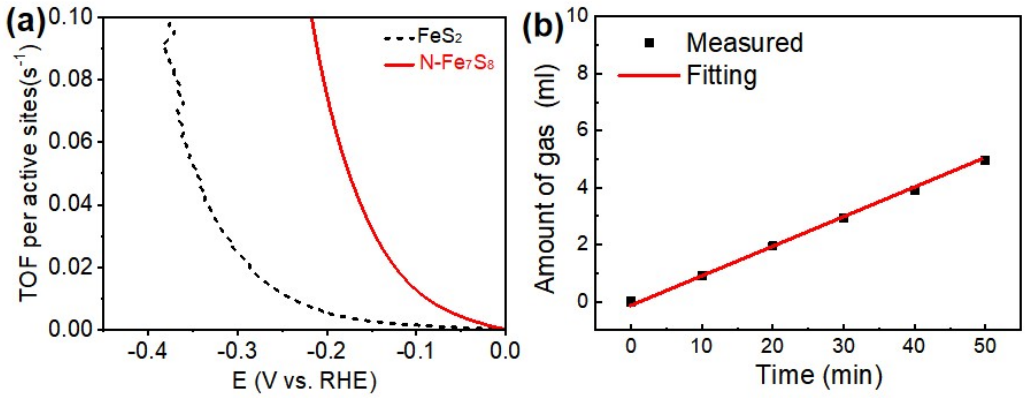

Figure S7. (a)TOF plots of FeS_2 and N-Fe_7S_8 with respect to the overpotential for HER, (b) the amount of theoretically calculated (red line) and experimentally measured gas versus time for N-Fe_7S_8 at a constant current density of 10 mA cm^{-2}.

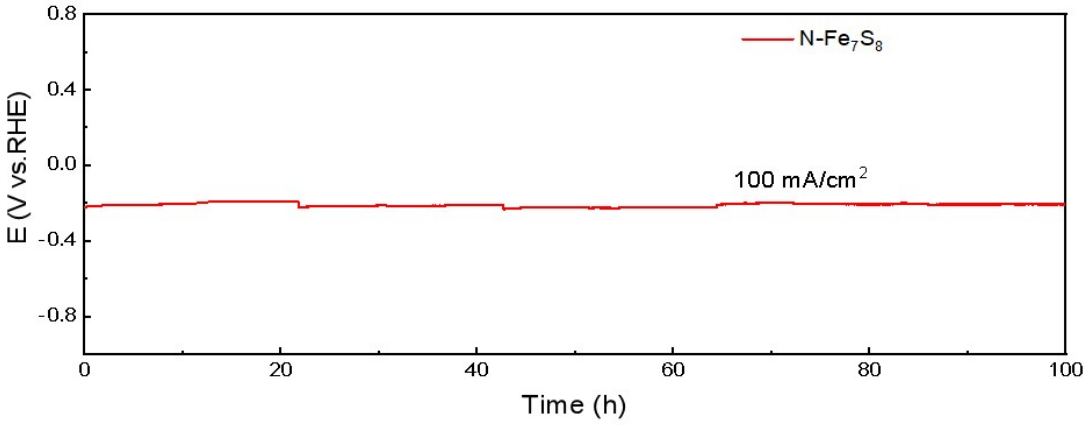

Figure S8. electrochemical stability of the N-Fe_7S_8@CC electrode.

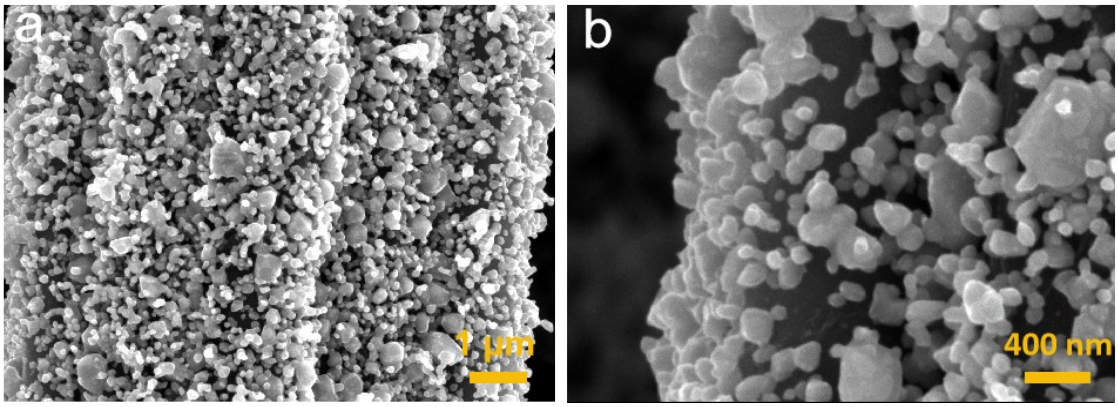

Figure S9. SEM images of N-Fe_7S_8 after the stability test.

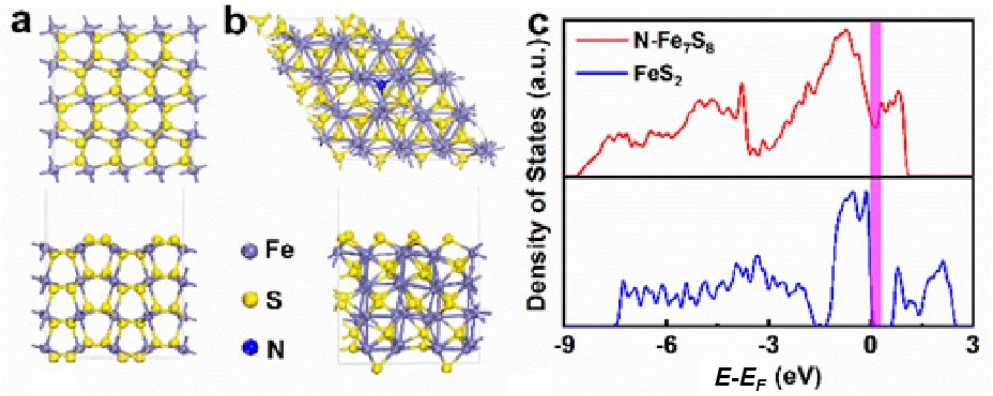

Figure S10. DFT calculation of FeS_2 and N-Fe_7S_8: (a-b) The optimized surface structures of FeS_2 and N-Fe_7S_8, respectively. (c) The total density of states (TDOS) of FeS_2 and N-Fe_7S_8.

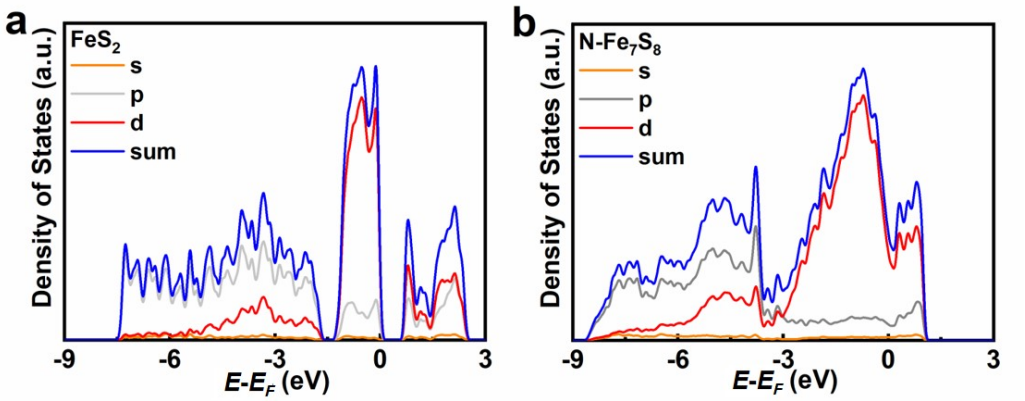

Figure S11. The calculated PDOS distribution of (a) FeS_2 and (b) N-Fe_7S_8, respectively.

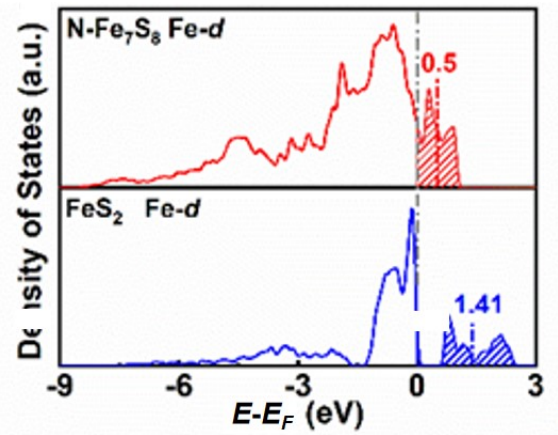

Figure S12. The detailed partial DOS (PDOS) distribution of the Fe d band in FeS_2 and N-Fe_7S_8.

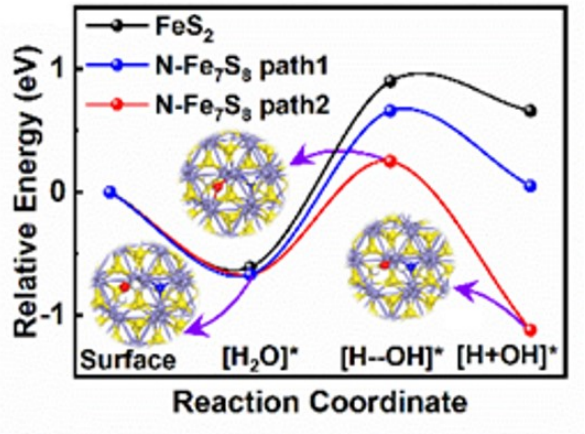

Figure S13. The relative energy diagram with simplified structural information along the reaction coordinate for water adsorption/dissociation on the surface of FeS_2 and N-Fe_7S_8.

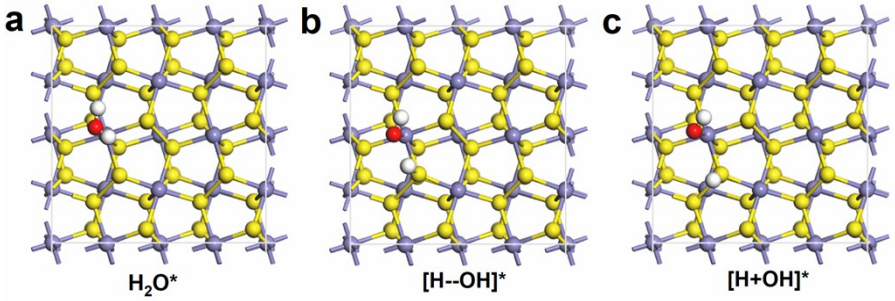

Figure S14. The optimized structural configurations for H_2O adsorption/dissociation on the surface of FeS_2.

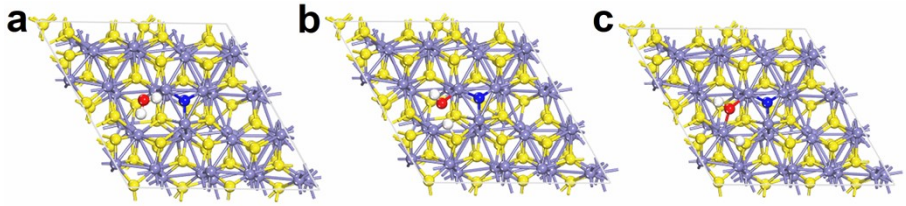

Figure S15. The optimized structural configurations for H_2O adsorption/dissociation on the surface of N-Fe_7S_8 (path1).

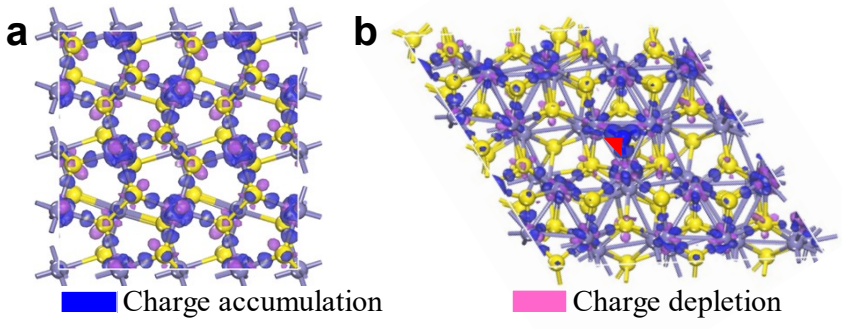

Figure S16. The 3D isosurface of electron density difference images of (a) FeS_2 and (b) N-Fe_7S_8.

Table S2. A performance comparison with recently published transition metal-based HER catalysts.

Material	HER η_{-10}(mV)	Tafel slope (mV dec^{-1})	Ref.
N-Fe_7S_8	89	105	This work
FeS/NiS/NF	144	39	[4]
FeS/Ni_3S_2@NF	130	124	[5]
Ni–Co–P/NF	156	108.4	[6]
Co_3S_4@FNC-Co_3	140	103	[7]
$NiCo_2S_4$/Ni_3S_2/NF	119	105.2	[8]
NF/T(Ni_3S_2/MnS-O)	116	41	[9]
δ-FeOOH/Ni_3S_2/NF	106	82.6	[10]
Fe-Mo-S/Ni_3S_2@NF	141	123	[11]
$NiWO_4$/Ni_3S_2	136	112	[12]
$CuFeS_2$/rGO	176	216	[13]

Refenerce

1. Y. Wu, X. Liu, D. Han, X. Song, L. Shi, Y. Song, S. Niu, Y. Xie, J. Cai and S. Wu, *Nature communications*, 2018, **9**, 1425.
2. N. Mardirossian and M. Head-Gordon, *The Journal of chemical physics*, 2015, **142**.
3. J. Linnera and A. Karttunen, *Physical Review B*, 2017, **96**, 014304.
4. R. Zhang, Z. Zhu, J. Lin, K. Zhang, N. Li and C. Zhao, *Electrochimica Acta*, 2020, **332**, 135534.
5. H. Li, S. Yang, W. Wei, M. Zhang, Z. Jiang, Z. Yan and J. Xie, *Journal of Colloid and Interface Science*, 2022, **608**, 536-548.
6. Y. Gong, Z. Xu, H. Pan, Y. Lin, Z. Yang and J. Wang, *Journal of Materials Chemistry A*, 2018, **6**, 12506-12514.
7. X. Zhu, J. Dai, L. Li, D. Zhao, Z. Wu, Z. Tang, L.-J. Ma and S. Chen, *Carbon*, 2020, **160**, 133-144.
8. H. Liu, X. Ma, Y. Rao, Y. Liu, J. Liu, L. Wang and M. Wu, *ACS applied materials & interfaces*, 2018, **10**, 10890-10897.
9. Y. Zhang, J. Fu, H. Zhao, R. Jiang, F. Tian and R. Zhang, *Applied Catalysis B: Environmental*, 2019, **257**, 117899.
10. X. Ji, C. Cheng, Z. Zang, L. Li, X. Li, Y. Cheng, X. Yang, X. Yu, Z. Lu and X. Zhang, *Journal of Materials Chemistry A*, 2020, **8**, 21199-21207.
11. Y. Zhang, H. Guo, X. Li, J. Du, W. Ren and R. Song, *Chemical Engineering Journal*, 2021, **404**, 126483.
12. S. Huang, Y. Meng, Y. Cao, F. Yao, Z. He, X. Wang, H. Pan and M. Wu, *Applied Catalysis B: Environmental*, 2020, **274**, 119120.
13. S. Swathi, R. Yuvakkumar, G. Ravi, M. Thambidurai, H. D. Nguyen and D. Velauthapillai, *ACS Applied Nano Materials*, 2023, **6**, 6538-6549.